



mm. This geometry corresponds to the one used in the experiments performed on a dry system [16]. In order to prevent the excitation of subharmonic modes, individual vertical taps were used to excite the system. Each tap consisted of one sinusoidal oscillation of frequency  $f$  and amplitude  $A_0$ ; its acceleration is characterized by a dimensionless parameter  $\Gamma = a_{\text{peak}}/g$ , where  $a_{\text{peak}} = (2\pi f)^2 A_0$  is the peak acceleration during a tap, and  $g = 9.8 \text{ m/s}^2$  is the Earth's gravitational acceleration. The excitation frequency ( $13 \leq f \leq 150$  Hz) and the acceleration ( $2.5 \leq \Gamma \leq 12$ ) ranges were determined by experimental constraints; the maximum accessible amplitude of shaking on one end of the range, and an acceptable duration of an experimental run on the other (as convection becomes immeasurably slow at high  $f$  and low  $\Gamma$ ).

While the container was being filled with granular material, colored tracer particles of diameter  $d_{\text{tracer}} = 3\text{--}4$  mm were inserted along the central axis of the system, at various depths from the surface  $z$ . As the system was vibrated, convective flow carried the tracer (along with other) particles to the surface, where they were observed using a video camera and a time-lapse recorder. We measured the number of taps  $t$  it took each particle, initially buried at depth  $z$ , to reach the surface, and refer to it as the dimensionless ‘‘time.’’

### III. RESULTS

Vertical vibrations induce convective flow in our system, established in the shape of a single convection roll, carrying the material upward in the center of the container and downward near the vertical walls. The convective flow in the bulk carries the tracer particles to the surface, where they become entrained in the downward flow along the walls and recirculated. When the convection rate is increased sufficiently, either by increasing  $\Gamma$  or decreasing  $f$ , the tracer particles, which have a larger diameter than the material particles, are not recirculated, but remain trapped at the top surface. When we replaced the frictional walls with smooth walls (i.e., the particles are not glued to the vertical container sides) the rise times of particles embedded deep in the bulk are approximately four times greater.

Figure 2 shows typical results of our  $z(t)$  measurements, done under the same experimental conditions ( $f = 30$  Hz,  $\Gamma = 6$ ) in a wet and a dry system, represented by the solid and open symbols, respectively. This data were taken with  $D = 103$  mm,  $h_0 = 200$  mm, and  $d = 3.7$  mm. Throughout the paper, the axes are oriented such that data from tracer particles with smaller initial depth  $z$  are plotted above particles with greater  $z$ , so that the progressively smaller values of  $z$  (from left to right of the plot) resemble a tracer particle's forward motion in time. Under the same experimental conditions, the rate of convection in a wet system is two orders of magnitude lower than in a dry system. (This is the reason that there are fewer data points in the curve for the wet than for the dry material.) This result is frequency dependent, and at  $f = 60$  Hz, the difference is reduced to one order of magnitude.

The  $z(t)$  data contain the information on the depth depen-

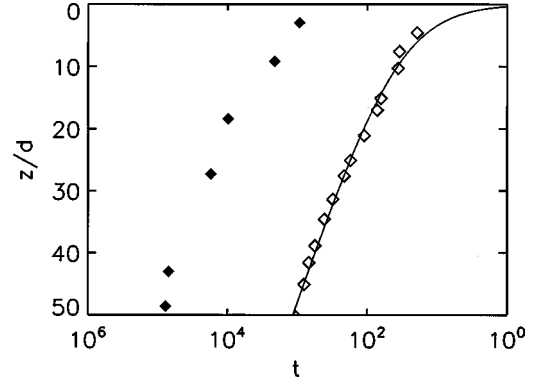


FIG. 2. Tracer bead rise times under wet and dry conditions. Two typical sets of measurement results are shown, taken under the same experimental conditions, in a wet (solid) and a dry (open symbols) system. The dimensionless time is measured in taps necessary to reach the surface at  $z = 0$ . The flow in the wet system is two orders of magnitude slower than in the dry system. These data were taken in a system with dimensions  $D = 103$  mm,  $h_0 = 200$  mm, and  $d = 3.7$  mm. The solid line is a fit to Eq. (1).

dence of  $v_c(z)$ , the upward convection velocity along the central axis of the system, where the tracer particles are introduced. In dry systems, an excellent fit to the data was obtained with a logarithmic form:

$$z = \xi \ln(1 + t/\tau) \quad (1)$$

which corresponds to

$$v_c(z) = (\xi/\tau) e^{-z/\xi}. \quad (2)$$

The solid line in Fig. 2 is a best fit of this form to the data taken in the dry system, and is shown for illustration. This fit yields two characteristic scales: the length scale  $\xi$ , describing the exponential decay of  $v_c(z)$ , and the time scale  $\tau$ , an inverse measure of the convection velocity. We can use this form to fit the data on the wet system as well. In Fig. 3 we show the dependence of  $\xi$  (in units of the bead diameter) and  $\tau$  on frequency  $f$  and acceleration  $\Gamma$ , as obtained from fits to the data taken in the wet system. Our results are compared to results taken from Ref. [16], of similar fits to data taken in an equivalent dry system, represented by the dashed lines. In a dry system, the length scale  $\xi$  was found to scale as the mechanical amplitude of vibration  $A_0$ , and hence the dashed lines describe a  $1/f^2$  dependence in frequency and linear growth in  $\Gamma$  [Figs. 3(a) and 3(b)]. Our results on the wet system are strikingly different; our data are consistent with  $\xi$  being independent of either  $f$  or  $\Gamma$ . It is possible that  $\xi$  even exhibits a weak growth upon increasing  $f$ , opposite to the trend observed in dry systems. The differences in the behavior of time scale  $\tau$  are less striking, being more quantitative in nature. Figure 3(c) shows that  $\tau$  grows approximately exponentially with  $f$  in both wet and dry systems, although at very different rates. In Fig. 3(d), even though within our experimental range we do not observe a divergence in  $\tau$ , we do observe a growing trend as  $\Gamma$  is decreased.

These differences between wet and dry systems suggest that there may be a different physical mechanism driving

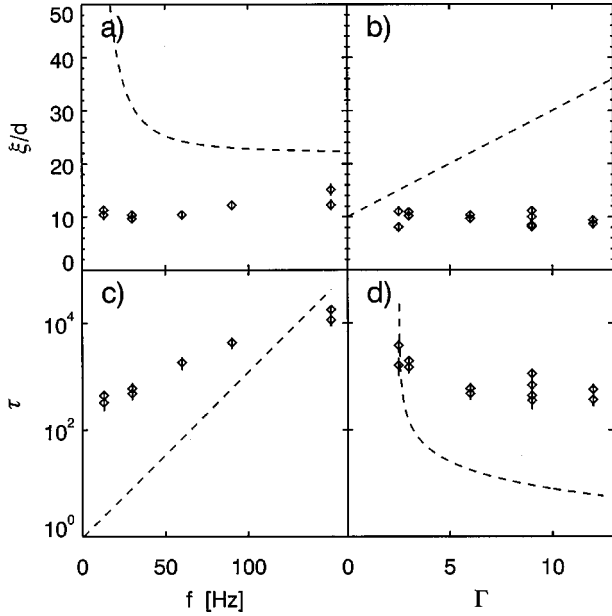


FIG. 3. Dependence for the wet system of the dimensionless fit parameters  $\xi/d$  and  $\tau$  in the logarithmic form [Eq. (1)] on  $f$  and  $\Gamma$ . While  $\xi/d$  does show a possible weak increase at high  $f$ , our data is consistent with  $\xi/d$  being largely independent on either  $f$  (a) or  $\Gamma$  (b);  $\tau$  grows exponentially with increasing  $f$  (c) and weakly with decreasing  $\Gamma$  (d). The dashed lines represent fits, taken from Ref. [16], to the  $\xi/d$  and  $\tau$  values obtained in an equivalent dry system. In (a), the dashed line follows a  $1/f^2$  dependence.

convection in the two cases. Indeed, we find that the logarithmic form for  $z(t)$ , appropriate for the dry material, may not provide the best fit to our wet-system data. Instead, we found that a power-law

$$z = At^p, \quad (3)$$

implying

$$v_c(z) = pA^{1/p}Z^{1-1/p} \quad (4)$$

gives a better fit to the data taken in the wet system. Figures 4(a) and 4(b) show a representative data set, taken at  $f = 30$  Hz and  $\Gamma = 6$ , fit to both the logarithmic and power-law

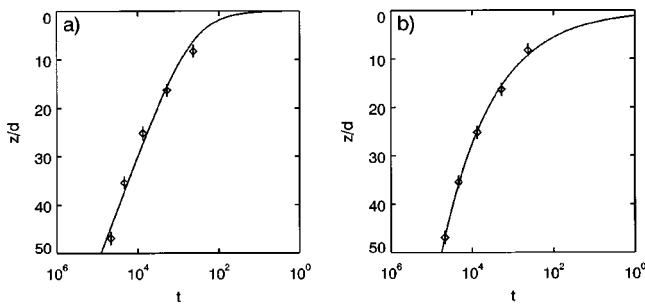


FIG. 4. Comparison of logarithmic and power-law fits. A data set taken at  $f = 30$  Hz and  $\Gamma = 6$  is plotted, and the best fit to the logarithmic (a) and the power-law form (b) are shown. The power-law form gives a better fit, as the logarithmic fit does not capture the curvature present in the data.

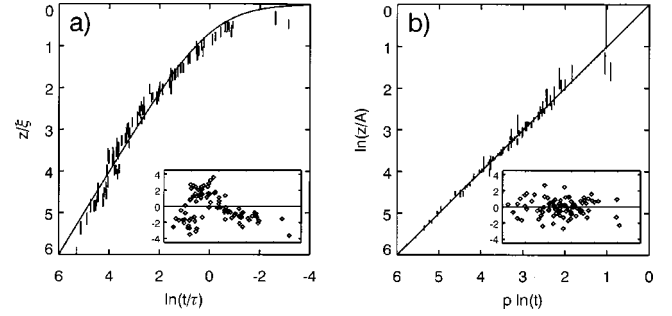


FIG. 5. Residual analysis for wet system data. (a) Best fits to the logarithmic functional form [Eq. (1)] are performed on data from 19 experimental runs. The scaled data show an imperfect collapse on the master curve (solid line). The inset shows the residuals for all performed fits, whose systematic clustering indicates that a better fit to the data is possible. Horizontal scale in the inset is identical to the horizontal scale in the main plot, and the vertical scale measures the deviation of the data points from the fit, normalized to the measurement uncertainty. (b) The same analysis, but using the power-law form [Eq. (3)], is performed on the data. The collapse on the master curve is better than in (a), evidenced by the random scatter of the residuals around zero.

functional forms, respectively. On the lin-log scale used, the logarithmic form asymptotes to a straight line at large values of  $z$  and  $t$ , and does not capture the curvature present in the data [Fig. 4(a)].

In order to get a better idea of how the two forms fit the data, we performed residual analysis on 19 experimental data sets, taken at various values of  $f$  and  $\Gamma$ . In Fig. 5(a), each experimental run is fit to the logarithmic form in Eq. (1), and the scaled depths  $z_s = z/\xi$  are plotted vs the logarithm of the scaled times  $t_s = t/\tau$ . The vertical bars represent the error in  $z_s$  due to the measurement uncertainty in  $z$ . The measurement error in  $t$  is negligible. If data are well fit by the functional form (given by the solid line), data from each experimental run should collapse onto that line. Our data, however, show significant systematic deviations; they lie below the functional form at small and large values of  $t_s$ , and above it in the intermediate range. The inset shows the residuals of the performed fits, normalized to the measurement uncertainty in  $z$ . The systematic clustering of the residuals away from zero indicates that a better fit to the data is possible. In Fig. 5(b) the same analysis is performed using the power-law form, and the appropriately scaled data are plotted on a log-log plot in order to obtain collapse on a straight line. We find that in this case the collapse is more satisfactory. The residuals, which are randomly distributed around zero, indicate a better fit to the data. When the same comparison is performed on the data taken by Knight *et al.* in a dry system [16], the logarithmic function is unambiguously found to be the superior fit. This analysis is shown in Fig. 6.

By fitting our experimental data to the power law given by Eq. (3), we obtain the values of parameters  $A$  and  $p$ , as a function of frequency  $f$  and peak acceleration  $\Gamma$ . The values of  $p$  obtained in this way are shown in Figs. 7(a) and 7(b). We find  $p = 0.37 \pm 0.02$  to be largely independent of either  $f$  or  $\Gamma$  (although there is a possibility that it increases weakly with frequency). When  $p$  is fixed to this value, and a one-

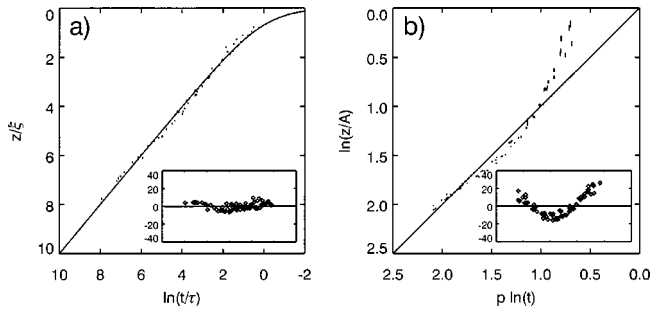


FIG. 6. Residual analysis for dry-system data obtained by Knight *et al.* (Ref. [16]). For comparison, the same analysis as for the wet material in Fig. 5 is shown here for data obtained on dry granular material. In contrast to the behavior found for wet material, a superior fit results from a logarithmic time dependence [Eq. (1)].

parameter fit for  $A$  is performed, less scatter is obtained than when  $p$  is allowed to vary. The results for  $A$  obtained in this way are shown in Figs. 7(c) and 7(d). In such a one-parameter fit,  $A$  corresponds directly to the rate of convection. From Fig. 7(c) we see that  $A$  decays logarithmically with  $f$ . In Fig. 7(d) a surprising result emerges; although  $A$  increases as  $\Gamma$  is increased, above  $\Gamma = 6$ ,  $A$  saturates. In contrast to observations made in the dry case, shaking the system harder does not enhance convection. Interestingly, it is also at  $\Gamma > 6$  that the (larger) tracer particles do not become entrained in the downward flow along the walls.

#### IV. CONCLUSIONS

We are unaware of any prior measurements of the convection velocity profile in a fully immersed, vertically vibrated granular system. We find that the convection is a robust phenomenon, and that it emerges with the same number and shape of convection rolls as does convection in a dry system.

The liquid does, however, affect the driving mechanism. In comparison with a dry system, the wet system flows up to two orders of magnitude more slowly than the dry one does. Presumably, lubrication of particle contacts results in reduced friction at the sidewalls and hence in weaker driving. In addition, we have evidence that another mechanism may contribute; when the frictional walls are substituted by smooth ones, the convection rate is reduced by approximately a factor of 4, but convection does not cease completely. By contrast, in a dry system, the use of smooth walls can bring convection almost to a standstill [17]. This result is not conclusive, however, as the friction against a rough and a smooth boundary could be comparable when both are lubricated.

We find additional evidence for a qualitatively different behavior in a wet and dry system. The different dependencies of  $\xi$  and  $\tau$  [in the logarithmic fit of  $z(t)$ ] on  $f$  and  $\Gamma$  are significant. Moreover, we find that the power-law depth de-

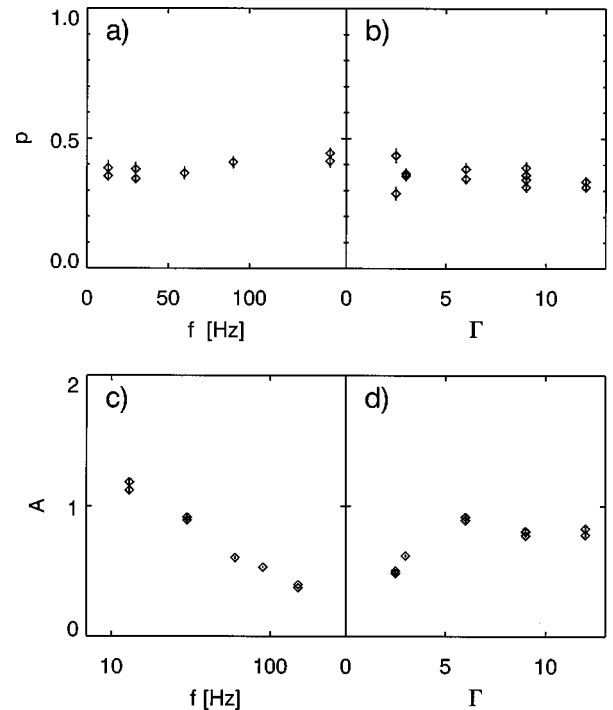


FIG. 7. Fit parameters to the power law. The exponent  $p$  in the power-law fit [Eq. (3)] is roughly independent of either (a)  $f$  or (b)  $\Gamma$ . We fix  $p$  to its average value of  $0.37 \pm 0.02$  and perform one-parameter fits for  $A$  [measured in units of the bead diameter, (d)], using the same equation.  $A$  decays logarithmically with increasing (c)  $f$ .  $A$  increases with increasing  $\Gamma$  up to (d)  $\Gamma = 6$ .

pendence of  $v_c(z)$  [Eq. (4)] is more appropriate for the wet system than the exponential one [Eq. (2)] observed in dry systems [16]. While the exponential fit of Eq. (2) yields a length and a time scale that describes the system behavior, the power-law fit gives no such scales, suggesting a different physical mechanism for the driving of the convection.

It is interesting to speculate that the new physical mechanism driving the convection is the hydrodynamic instability first discussed by Faraday in 1831 [8] and most recently studied in the context of heaping by Pak *et al.* [9]. In that instability, the interstitial fluid, which must flow to the container bottom in order to fill any unoccupied space when the granular material is moving upward, can entrain particles in its flow down the container walls. Further studies are necessary in order to ascertain whether this mechanism indeed contributes to the driving of convection in the wet systems.

#### ACKNOWLEDGMENTS

The authors would like to thank James B. Knight on helpful discussions. This work was supported by the NSF under Contract No. CTS-9710991 and by the MRSEC Program of the NSF under Contract No. DMR-9808595.

- [1] R. A. Bagnold, Proc. R. Soc. London, Ser. A **225**, 49 (1954).
- [2] S. A. Altobelli, E. Fukushima, and L. A. Mondy, J. Rheol. **41**, 1105 (1997).
- [3] P. Coussot and C. Ancey, Phys. Rev. E **59**, 4445 (1999).
- [4] S. P. Meeker, W. C. K. Poon, and P. N. Pusey, Phys. Rev. E **55**, 5718 (1997).
- [5] A. Ivanova, V. Kozlov, and P. Evesque, Europhys. Lett. **35**, 159 (1996).
- [6] V. G. Kozlov, A. A. Ivanova, and P. Evesque, Europhys. Lett. **42**, 413 (1998).
- [7] A. Stegner, and J. E. Wesfreid, Phys. Rev. E **60**, 3487 (1999).
- [8] M. Faraday, Philos. Trans. R. Soc. London **52**, 299 (1831).
- [9] H. K. Pak, E. V. Doorn, and R. P. Behringer, Phys. Rev. Lett. **74**, 4643 (1995).
- [10] S. Nasuno, A. Kudrolli, and J. P. Gollub, Phys. Rev. Lett. **79**, 949 (1997).
- [11] J.-C. Géminard, W. Losert, and J. P. Gollub, Phys. Rev. E **59**, 5881 (1999).
- [12] R. Albert, I. Albert, D. Hornbaker, P. Schiffer, and A.-L. Barabási, Phys. Rev. E **56**, 6271 (1997).
- [13] T. G. Mason, A. J. Levine, D. Ertas, and T. C. Halsey, Phys. Rev. E **60**, 5044 (1999).
- [14] P. Tegzes, R. Albert, M. Paskvan, A.-L. Barabási, T. Vicsek, and P. Schiffer, Phys. Rev. E **60**, 5823 (1999).
- [15] G. D'Anna, Europhys. Lett. **51**, 293 (2000).
- [16] J. B. Knight, E. E. Ehrichs, V. Y. Kuperman, J. K. Flint, H. M. Jaeger, and S. R. Nagel, Phys. Rev. E **54**, 5726 (1995). We found a typographical error in the numbers describing these fits: we find the correct values to be  $f_0=14$  Hz,  $\Gamma_c=2.5$ , and  $\beta=1.1$ .
- [17] J. Knight (private communication).